

**This is an electronic reprint of the original article.
This reprint *may differ* from the original in pagination and typographic detail.**

Author(s): Johansson, Andreas; Myllyperkiö, Pasi; Koskinen, Pekka; Aumanen, Jukka;
Koivistoinen, Juha; Tsai, Hung-Chieh; Chen, Chia-Hao; Chang, Lo-Yueh; Hiltunen, Vesa-
Matti; Manninen, Jyrki; Woon, Wei-Yen; Pettersson, Mika

Title: Optical Forging of Graphene into Three-Dimensional Shapes

Year: 2017

Version:

Please cite the original version:

Johansson, A., Myllyperkiö, P., Koskinen, P., Aumanen, J., Koivistoinen, J., Tsai, H.-C.,
Chen, C.-H., Chang, L.-Y., Hiltunen, V.-M., Manninen, J., Woon, W.-Y., & Pettersson,
M. (2017). Optical Forging of Graphene into Three-Dimensional Shapes. *Nano
Letters*, 17(10), 6469-6474. <https://doi.org/10.1021/acs.nanolett.7b03530>

All material supplied via JYX is protected by copyright and other intellectual property rights, and duplication or sale of all or part of any of the repository collections is not permitted, except that material may be duplicated by you for your research use or educational purposes in electronic or print form. You must obtain permission for any other use. Electronic or print copies may not be offered, whether for sale or otherwise to anyone who is not an authorised user.

Optical Forging of Graphene into Three-Dimensional Shapes

Andreas Johansson, Pasi Myllyperkiö, Pekka Koskinen, Jukka Aumanen,
Juha Tapio Koivistoinen, Hung-Chieh Tsai, Chia-Hao Chen, Lo-Yueh Chang,
Vesa-Matti Hiltunen, Jyrki Manninen, Wei-Yen Woon, and Mika Pettersson

Nano Lett., **Just Accepted Manuscript** • DOI: 10.1021/acs.nanolett.7b03530 • Publication Date (Web): 19 Sep 2017

Downloaded from <http://pubs.acs.org> on September 21, 2017

Just Accepted

“Just Accepted” manuscripts have been peer-reviewed and accepted for publication. They are posted online prior to technical editing, formatting for publication and author proofing. The American Chemical Society provides “Just Accepted” as a free service to the research community to expedite the dissemination of scientific material as soon as possible after acceptance. “Just Accepted” manuscripts appear in full in PDF format accompanied by an HTML abstract. “Just Accepted” manuscripts have been fully peer reviewed, but should not be considered the official version of record. They are accessible to all readers and citable by the Digital Object Identifier (DOI®). “Just Accepted” is an optional service offered to authors. Therefore, the “Just Accepted” Web site may not include all articles that will be published in the journal. After a manuscript is technically edited and formatted, it will be removed from the “Just Accepted” Web site and published as an ASAP article. Note that technical editing may introduce minor changes to the manuscript text and/or graphics which could affect content, and all legal disclaimers and ethical guidelines that apply to the journal pertain. ACS cannot be held responsible for errors or consequences arising from the use of information contained in these “Just Accepted” manuscripts.



Optical Forging of Graphene into Three- Dimensional Shapes

*Andreas Johansson^{1,2} †, Pasi Myllyperkiö¹ †, Pekka Koskinen², Jukka Aumanen¹, Juha Koivistoinen¹, Hung-Chieh Tsai³, Chia-Hao Chen⁴, Lo-Yueh Chang⁴, Vesa-Matti Hiltunen², Jyrki J. Manninen², Wei Yen Woon³, Mika Pettersson¹ **

¹Nanoscience Center, Department of Chemistry, P.O. Box 35, FI-40014, University of Jyväskylä, Finland.

²Nanoscience Center, Department of Physics, P.O. Box 35, FI-40014, University of Jyväskylä, Finland.

³Department of Physics, National Central University, Jungli, 32054, Taiwan, Republic of China.

⁴National Synchrotron Radiation Research Center, Hsinchu, 30076, Taiwan, Republic of China.

Abstract: Atomically thin materials, such as graphene, are the ultimate building blocks for nanoscale devices. But although their synthesis and handling today are routine, all efforts thus far have been restricted to flat natural geometries, since the means to control their three-dimensional (3D) morphology has remained elusive. Here we show that, just as a blacksmith uses a hammer to forge a metal sheet into 3D shapes, a pulsed laser beam can forge a graphene sheet into

1
2
3 controlled 3D shapes in the nanoscale. The forging mechanism is based on laser-induced local
4 expansion of graphene, as confirmed by computer simulations using thin sheet elasticity theory.
5
6
7

8
9
10 **Keywords:** graphene, strain-engineering, femtosecond laser, defects, 3-dimensional, elasticity
11 modeling
12
13

14
15 Graphene, a single atomic layer of carbon, is the most studied 2D material and is characterized
16 by excellent carrier mobility, strength, flexibility, transparency and constant absorption in a
17 broad range of the electromagnetic spectrum, making graphene an excellent material for novel
18 applications in electronics, photonics and optoelectronics.^{1,2} Examples of reported devices
19 include sensors, field effect transistors (FET), supercapacitors and photodetectors.³ Graphene is
20 not strictly planar but contains corrugations, wrinkles, ripples and other out-of-plane
21 deformations.⁴ These structural changes provide a way to modify the electronic properties of
22 graphene but controlling them is challenging.⁵⁻⁸ So far, modification of the third dimension of
23 graphene has relied on spot-blistering, substrate molding or strain-induced periodic modulation,
24 as well as cutting graphene or connecting graphene flakes with functional groups, while
25 controlled shaping of graphene itself into more complex custom-made 3D architectures has
26 remained elusive.⁹⁻¹³
27
28
29
30
31
32
33
34
35
36
37
38
39
40
41
42

43 Here, we demonstrate the forging of graphene into free-standing 3D shapes by exploiting local
44 strain induction due to irradiation with femtosecond laser pulses under inert atmosphere. While
45 laser irradiation in air has earlier been shown to generate two-photon functionalization of the
46 graphene surface with oxygen containing groups,¹⁴ we argue here that the inert atmosphere
47 allows a fundamentally different process of defect engineering to take place. Computer
48 simulations using elasticity theory confirm experimental observations and provide the theoretical
49
50
51
52
53
54
55
56
57
58
59
60

1
2
3 basis for the method. The optical forging opens new possibilities for fundamental studies and for
4
5 the development of applications based on 3D shapes of graphene.
6
7

8 We patterned single-layer graphene on a Si/SiO₂ substrate by direct laser writing with tightly
9
10 focused femtosecond pulses under nitrogen and argon atmospheres, which both produced
11
12 qualitatively similar results. A matrix of 2 x 2 μm² squares was patterned on graphene. Each
13
14 square was irradiated by 441 partially overlapping spots at 100 nm spot separation. The
15
16 irradiation time per spot was varied from 0.1 s to 2.0 s. Surprisingly, the irradiated squares
17
18 formed elevated flat plateaus with sharp boundaries, as seen in atomic force microscope (AFM)
19
20 images (Figure 1a). The height varies from ~3 nm up to ~20 nm (Figure 1b) and is proportional
21
22 to the square root of irradiation time (Supporting Information, Figure S1). This proportionality
23
24 can be theoretically justified, as shown later. We didn't observe any wrinkling on the plateaus or
25
26 just outside them, except for folding already present in graphene before patterning. Remarkably,
27
28 the patterned matrix is well visible under an optical microscope due to enhanced reflection of the
29
30 irradiated areas (Figure 1c). With increasing irradiation time, the brightness of the irradiated
31
32 spots increases and the color changes from greenish towards yellow.
33
34
35
36
37
38
39
40
41
42
43
44
45
46
47
48
49
50
51
52
53
54
55
56
57
58
59
60

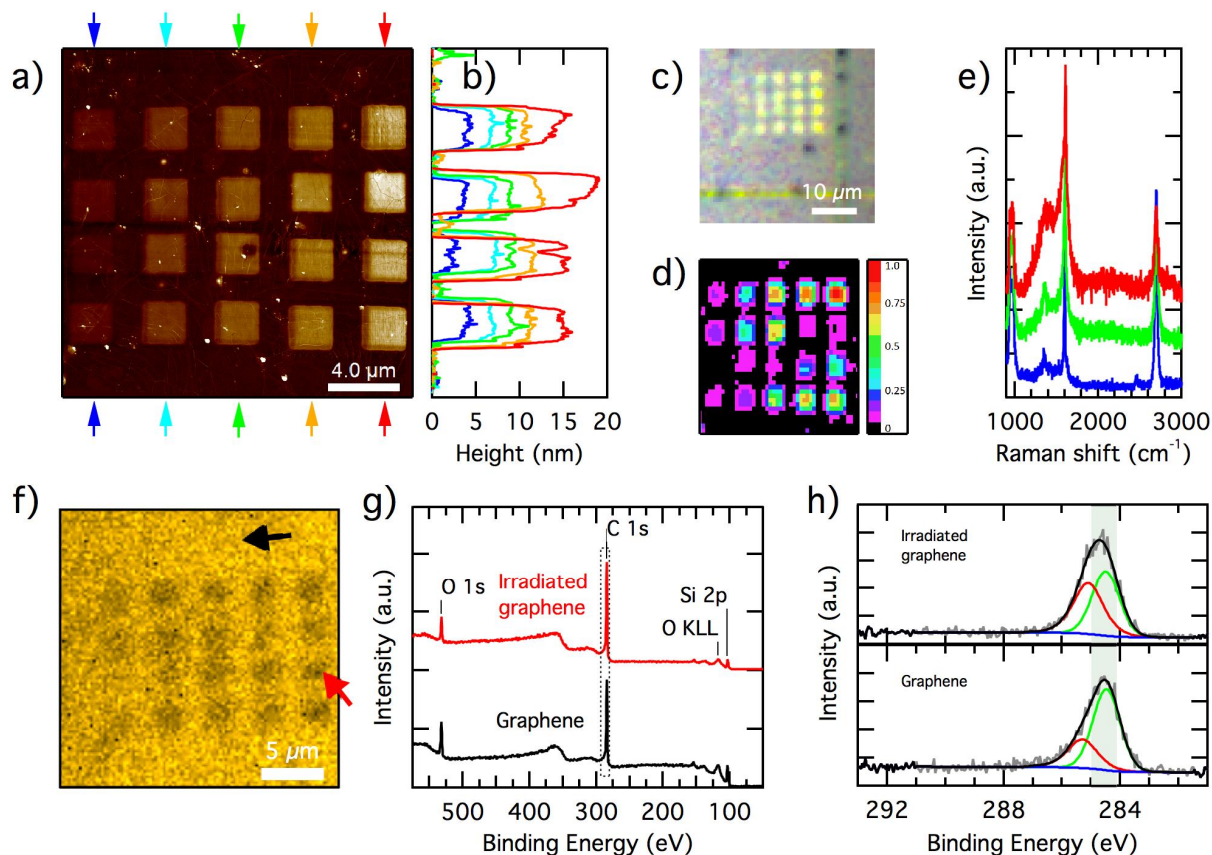


Figure 1. Characterization of irradiated graphene. a) AFM image. b) Line profiles of the AFM image between the arrows, shown in a. c) Optical microscope image. The lines on the bottom and right are a part of the 30 nm thick and 1 μm wide gold reference grid. d) Raman map showing integrated intensity in the D-band area at $\sim 1350\text{ cm}^{-1}$. e) Raman spectra measured from graphene with no irradiation (bottom) and with 0.5 s (middle) and 2 s (top) of irradiation per spot. f) XPS image of the C1s signal at 285.0 – 284.2 eV. g) XPS survey spectra of non-irradiated graphene (bottom) and irradiated graphene (top). h) XPS C1s spectra of non-irradiated area (bottom; black arrow in f) and irradiated area (top; red arrow in f). The shaded area shows the region used to construct the image in f. The grey line shows the raw spectrum, black line is the fit that contains components of C=C (green), C-C (red) and background (blue).

The squares are visible in a Raman map of the integrated intensity of the D-band including the contribution from the overlapping broad emission, which increases with irradiation (see Figures 1d and e). While local variations are observed, there is an overall trend towards increased integrated intensity with increased irradiation time. The characteristic spectrum of non-irradiated

1
2
3 graphene (Figure 1e, bottom) is observed also in the irradiated areas (Figure 1e, middle and top).
4
5 Note that the Raman spectrum of non-irradiated graphene does not show any significant presence
6
7 of amorphous carbon, which excludes amorphous carbon redeposition or exfoliation¹⁵ as the
8
9 cause for the elevated plateaus. With increasing irradiation dose, broadened G- and D-bands
10
11 develop while the normal Raman spectrum of (non-irradiated) graphene remains (Figure 1e). The
12
13 total spectrum is thus a sum of two components: normal and broad (additional Raman spectra are
14
15 shown in Supporting Information, Figure S2). The broad spectrum resembles highly disordered
16
17 graphene but there is no growth of a sharp D-band, which is a characteristic signature of
18
19 scattered point defects in graphene.^{16,17} These observations suggest that irradiation transforms
20
21 local regions of graphene into disordered form. In Raman spectra, also a broad emission
22
23 background emerges upon irradiation (seen as a rising background in Figure 1e).
24
25
26
27
28

29 The sample was imaged by X-ray photoelectron spectroscopy (XPS) at sub-micrometer spatial
30
31 resolution (Figure 1f). XPS did not reveal significant change in the chemical composition of
32
33 graphene irradiated under nitrogen atmosphere (Figure 1g). Yet, contrast is found in scanning
34
35 photoelectron microscopy due to overall lower XPS intensity for patterned areas (Figure 1f).
36
37 The carbon C1s peak becomes broader towards the higher binding energy tail, indicating
38
39 decrease in the sp^2 C=C bond and increase in the C-C bond density (Figure 1h). The XPS data is
40
41 consistent with the defect generation picture as deduced from Raman spectra. The lack of oxygen
42
43 containing groups again supports the notion that amorphous carbon does not contribute to the
44
45 elevated plateaus. For comparison, irradiation of the same sample with analogous patterns under
46
47 air reveals characteristic signals of oxidized carbon (Supporting Information, Figure S3).^{14,18,19}
48
49
50
51
52
53
54
55
56
57
58
59
60

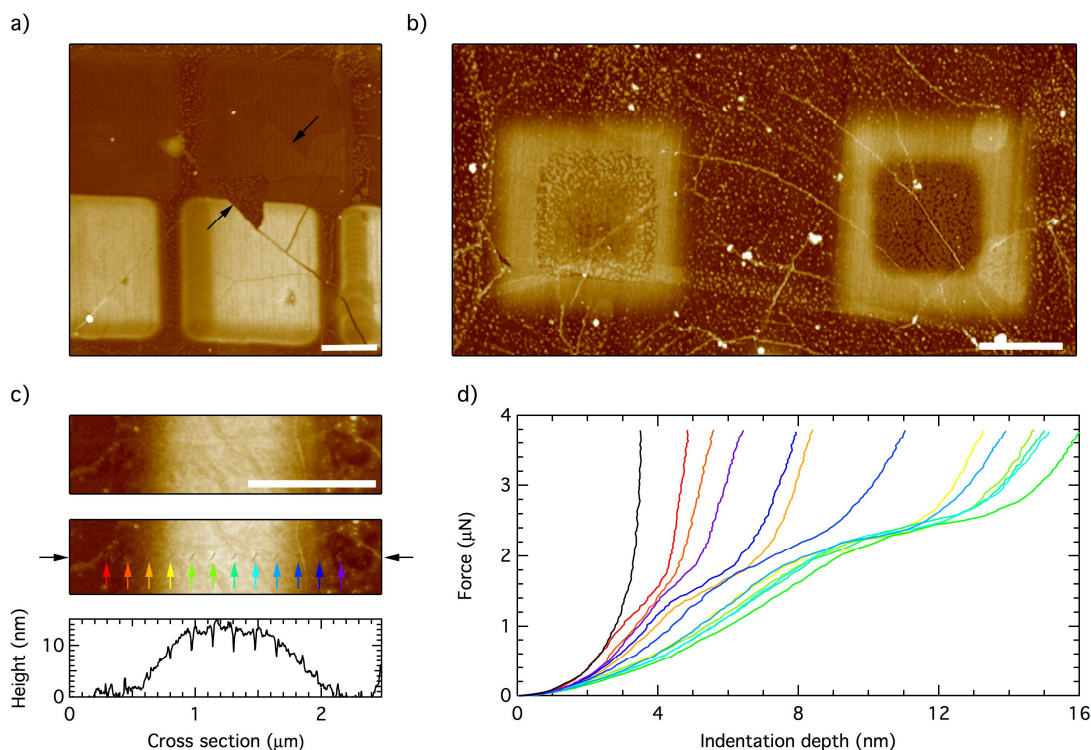


Figure 2. a) AFM image of squares patterned under air (top) and nitrogen (bottom). The arrows point out where a triangular shaped section of graphene has folded. b) AFM image of large squares patterned under nitrogen, with center regions in addition patterned under air. The center region was patterned after the larger square for the left pattern and before the larger square for the right pattern. c) AFM data from nanoindentation area, showing topography before (top pane) and after (middle pane). The cross section (bottom pane) is taken between the black arrows in the middle pane. d) Nanoindentation data showing the measured force versus indentation depth. The trace colors correspond to the arrow colors in c showing the measurement location, except for the black trace, which is measured on bare SiO_2 . All scale bars are 1 μm .

To further investigate the nature of the elevated plateaus we prepared a series of square patterns and compared them to square patterns made under air. In Figure 2a, two rows of squares patterned on graphene are presented. The barely visible top row was patterned under air, leading to functionalization of the surface with mainly epoxy and hydroxyl groups.^{14,19} The height of the squares is about 1.3 nm. The bottom row was patterned under nitrogen, leading to elevated plateaus of about 20 nm in height. At the center of the image there is a triangular-shaped area in which the graphene has folded towards the upper right corner. In that area, no pattern is formed

1
2
3 under either oxygen or nitrogen atmosphere, and the surface seems unaffected by the laser
4 exposure. This observation again refutes that amorphous carbon deposition would contribute to
5 the elevated plateaus. Additionally, it refutes the possibility of formation of elevated plateaus due
6 to swelling of the underlying SiO₂ substrate.^{20,21} Folds, cracks and other surface features on
7 graphene continue from the areas outside the plateaus to the inside. This is strong additional
8 evidence that deposition of material cannot be responsible for the elevated features.
9

10
11 Figure 2b shows two square patterns prepared by combining laser patterning under both air and
12 nitrogen. For the left square pattern, first the large 2x2 μm² square was patterned under nitrogen,
13 forming a 6 nm high plateau. Then the inner 1x1 μm² square was patterned under air. The inner
14 square is somewhat crumpled with an average height of 3.5 nm. For the right square pattern, first
15 the inner 1x1 μm² square was patterned under air, and the outer 2x2 μm² square patterned under
16 nitrogen. Here the inner square has a height of 1.3 nm, which is similar to oxidized areas in
17 Figure 2a. The outer frame is again 6 nm high. The data shows that functionalization of the
18 graphene surface with oxygen containing groups leads to suppression of elevated plateau
19 formation.
20
21
22
23
24
25
26
27
28
29
30
31
32
33
34
35
36
37

38 We also performed AFM nanoindentation across a 12 nm high, 1 μm wide and 6 μm long
39 graphene plateau. The nanoindentation area is shown in Figure 2c before (top) and after
40 indentation (middle), together with a cross section (bottom) along the indentation line. The
41 measured force versus indentation depth curves are shown in Figure 2d, with color
42 corresponding to the arrows in Figure 2c pointing out their measurement locations. The resulting
43 force versus indentation depth curves show initially a non-linear increase, with a much weaker
44 response than indentation on bare SiO₂ surface (black trace). At around 2 μN a plateau develops,
45 which is interpreted as the graphene feature buckling towards the surface. It is interesting to note
46
47
48
49
50
51
52
53
54
55
56
57
58
59
60

1
2
3 that this force is very similar to the nanoindentation force at which suspended graphene
4 membranes break.^{22,23} The force curve then increases again with a dependence similar to that of
5
6 indentation on a bare SiO₂ surface. The onset of the second increase corresponds well to the
7
8 height of the graphene structure, indicating that the onset corresponds to the tip reaching the SiO₂
9
10 surface. The AFM image taken after nanoindentation (Figure 2c, middle) shows that the
11
12 graphene structure has returned to its original shape, except for piercing marks where the AFM
13
14 probe was indenting the surface.
15
16
17
18

19
20 All the evidence taken together suggests that irradiation under inert atmosphere leads to the
21
22 formation of elevated graphene structures containing only carbon. The most plausible
23
24 explanation for the underlying driving force is that, by analogy to the blister formation in
25
26 polymers, photons modify the lattice and induce local expansion of graphene.
27
28

29
30 To investigate this hypothesis, we used thin sheet elasticity theory to model expanded and
31
32 deformed graphene (see Supporting Information). We assumed that, via a mechanism discussed
33
34 later, the laser-induced lattice expansion field $\epsilon(\mathbf{r})$ is proportional to the spatial irradiation dose
35
36 $I(\mathbf{r})$. The spatial dependency was adopted from experimental input in conjunction with a
37
38 Gaussian beam profile (full width at half maximum, FWHM=500 nm).¹⁸ The maximum strain
39
40 $\epsilon_0 = \max[\epsilon(\mathbf{r})]$ was chosen and the topography was searched for by structural optimization. As a
41
42 result, simulation of a $2 \times 2 \text{ } \mu\text{m}^2$ pattern with $\epsilon_0 \gg 4.5 \times 10^{-5}$ gave topography and dimensions
43
44 in perfect agreement with the experiments (Figures 3a, b). The agreement is the first indication
45
46 suggesting that local expansion indeed is the driving force behind the observed structures.
47
48
49
50

51
52 The plateau formation can be understood simply in terms of increased surface area.
53
54 Geometrical considerations provide an estimate for the height of a $L_0 \times L_0$ square pattern as
55

$$56 \quad h(\epsilon_0) = \sqrt{0.81\epsilon_0 w(L_0 + 1.1 \times FWHM)}, \quad (1)$$

57
58
59
60

where w is the edge width (see Supporting Information). We simulated the $2 \times 2 \text{ mm}^2$ pattern with expansions up to $\epsilon_0 = 1\%$ and observed that Eq. (1) with $w \gg 3 \times FWHM$ captures well the dependence of height on strain (Figure 3c). Especially the square root dependence indicates how modest expansions are able to trigger notable structures. By inverting Eq. (1) and using the experimental data for $h(t)$ we could plot $\epsilon_0(t)$, the expansion as a function of time (Supporting Information, Figure S4). The plot shows that strain grows linearly with irradiation time, here at rates around $\sim 0.01\%$ per second.

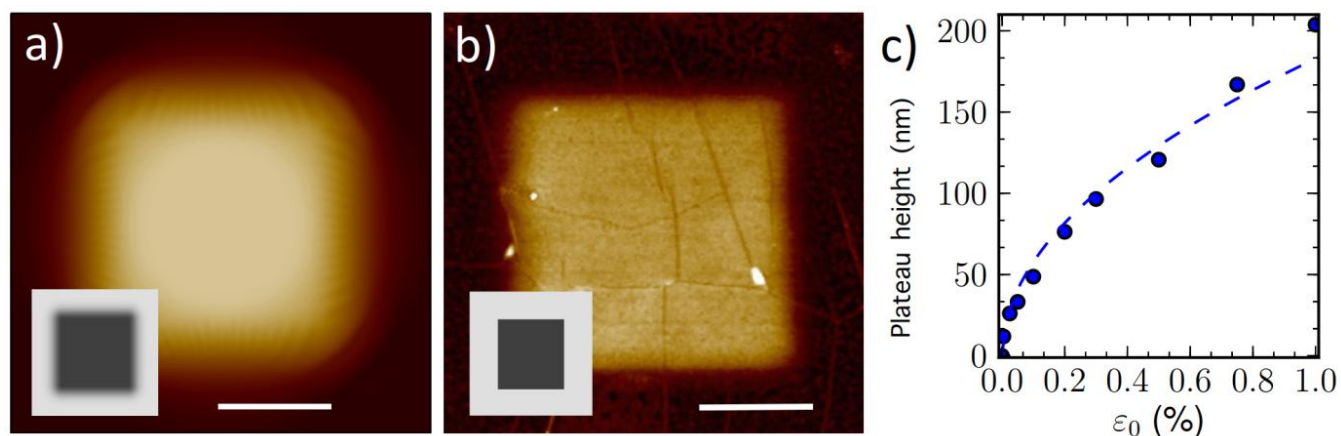


Figure 3. Elasticity modeling of plateau formation by local expansion. a) Optimized topography of a simulated $2 \times 2 \text{ mm}^2$ square pattern. Inset: the input strain field $\epsilon(\mathbf{r})$; maximum strain is $\epsilon_0 = 4.5 \times 10^{-5}$. b) AFM topography of the plateau (corresponding to 1.5 s irradiation time in Figure 1a). The plateau height is 12 nm in both simulation and experiment. Inset: bitmap image used for laser writing. Scale bars, 1 mm . c) Simulated height of $2 \times 2 \text{ mm}^2$ square plateaus at different ϵ_0 ; the dashed line is Eq. (1).

The most plausible mechanism for the expansion mechanism is irradiation-induced defect formation. Raman spectra indicate that irradiation produces disordered regions (Figure 1e). It is

1
2
3 reasonable to assume that in the beginning of the process, isolated defects are formed. The
4 density of isolated point defects can be estimated from the I(D)/I(G) ratio.²⁴ Our non-irradiated
5 CVD-grown graphene sample shows a ratio of ~ 0.1 , corresponding to an initial defect density \sim
6 10^{11} cm⁻² (Figure 1e).²⁴ Since the sharp D-band does not grow significantly in irradiation, the
7 point defect density does not grow much beyond $\sim 10^{11}$ cm⁻². Yet, because the lattice nevertheless
8 expands, after the initial formation of scattered point defects, the expansion must be driven
9 mainly by growth of isolated disordered regions. To investigate this possibility, we simulated
10 mean lattice expansion due to repulsive point defects at various densities and strengths of
11 influence (Figure 4a). Simulations show that $h \lesssim 20$ nm structures ($\epsilon_0 \lesssim 0.01\%$) can be created
12 by defect densities $\sim 10^{11} - 10^{12}$ cm⁻² and $h \gg 1$ nm structures ($\epsilon_0 \sim 3 \times 10^{-5} \%$) by defect
13 densities $\sim 10^9$ cm⁻². This explains why elevated structures can be formed already at defect
14 densities not visible in the Raman spectra.
15
16
17
18
19
20
21
22
23
24
25
26
27
28
29
30
31
32

33 The situation at longer irradiation times is different. Prolonged single spot irradiation created a
34 ~ 1.2 - μ m-diameter, 150-nm-high structure (Figure 4b). Measurement of the surface area
35 indicated $\epsilon_0 = 5\%$ expansion, assuming saturated expansion throughout the structure. Its
36 stability was confirmed also in the simulation (Figure 4c). Most important, its Raman spectrum
37 shows dominantly broad features, which is consistent with having highly disordered graphene
38 (Figure 4d). Strains in the 5 % range require defect densities above 10^{14} cm⁻² (Figure 4a), which
39 is in accordance with Raman spectra at high defect density.²⁴ At intermediate irradiations, the
40 coexistence of normal and broad spectra can be understood by assuming that defects form
41 preferentially in the vicinity of pre-existing defect regions that remain separated. As defect
42 regions grow and finally coalesce at densities $\sim 10^{14} - 10^{15}$ cm⁻², the entire irradiated area
43
44
45
46
47
48
49
50
51
52
53
54
55
56
57
58
59
60

becomes disordered and yields a completely broad Raman spectrum (see illustrative schematic in Supporting Information, Figure S5).

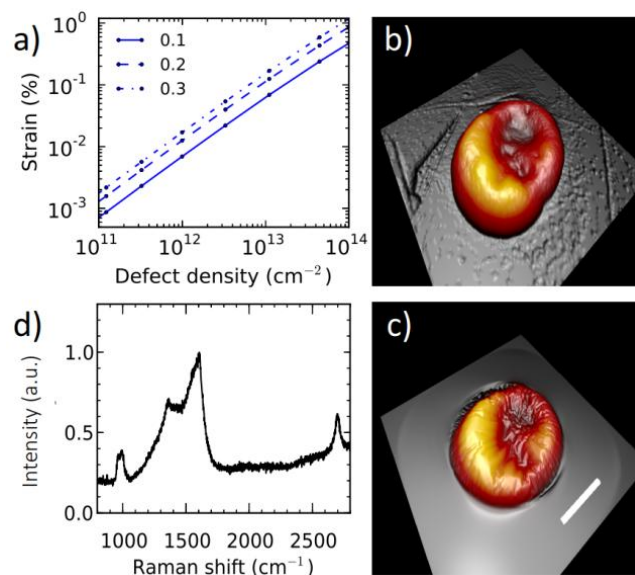


Figure 4. Point defects as the mechanism behind local expansion. a) Averaged strain in graphene as a function of density of point defects, calculated using the elastic model with 2.5 Å grid spacing. The three different defect strengths of influence stand for the strain in the defected lattice point. b) Experimentally observed, a 150 nm high partially collapsed structure resulting from prolonged irradiation at one spot. c) Simulated and optimized structure corresponding to panel b ($\epsilon_0 = 5\%$ within the structure). Vertical dimensions in b and c are scaled by factor of two; scale bar, 0.5 μm . d) Raman spectrum of the collapsed structure.

We lack direct evidence for the atomic structure of the defect, but let us consider one promising candidate—the bond rotation or Stone-Wales (SW) defect.²⁵ It is a fitting defect type because it requires no additional atoms, its formation energy of 4.6 – 5.7 eV²⁵ is close to the two-photon energy of 4 – 5 eV in experiments, and it causes expansion of suitable magnitude at

1
2
3 suitable defect densities (Figure 4a and Supporting Information, Figure S6). Moreover, the SW
4 defects have attractive interaction and can gradually develop into extended Haeckelite structures
5 that consist of arrangements of pentagons, hexagons and heptagons.^{26,27} For example, the most
6 stable Haeckelite, $H_{5,6,7}$, is 3 % less dense than graphene, which is in rough agreement with the
7 experimental saturation strain of 5 % (Figure 4b).²⁸ Haeckelites are also metallic, which matches
8 with the increased reflectance within the structures (Figure 1c).²⁷ While other mechanisms such
9 as thin film interference could as well contribute to increased optical response,^{29,30} SW defects
10 and Haeckelite structures stand out as promising candidates to explain both increased reflectance
11 and lattice expansion, although confirmation requires further studies.
12
13
14
15
16
17
18
19
20
21
22
23

24 After establishing the method and mechanism for 3D patterning we describe fabrication of
25 more complex 3D structures. The first example is a pyramid structure (Figure 5a). The pyramid
26 was fabricated by first making the base level and then building the next levels step-wise (profile
27 in Figure 5b). Such a pyramid was confirmed to be stable also in simulation (Figure 5, inset).
28 The pyramid is a fascinating demonstration of the possibility to repeat the structure formation on
29 previously formed flat structure – such progressive control enables building arbitrarily complex
30 architectures. In addition, we fabricated a 150-nm-high round semi-sphere, which had collapsed
31 symmetrically, a miniature grating, a chiral structure (spiral), a matrix of squares, and a torch
32 (Figures 5c – g).
33
34
35
36
37
38
39
40
41
42
43
44
45
46
47
48
49
50
51
52
53
54
55
56
57
58
59
60

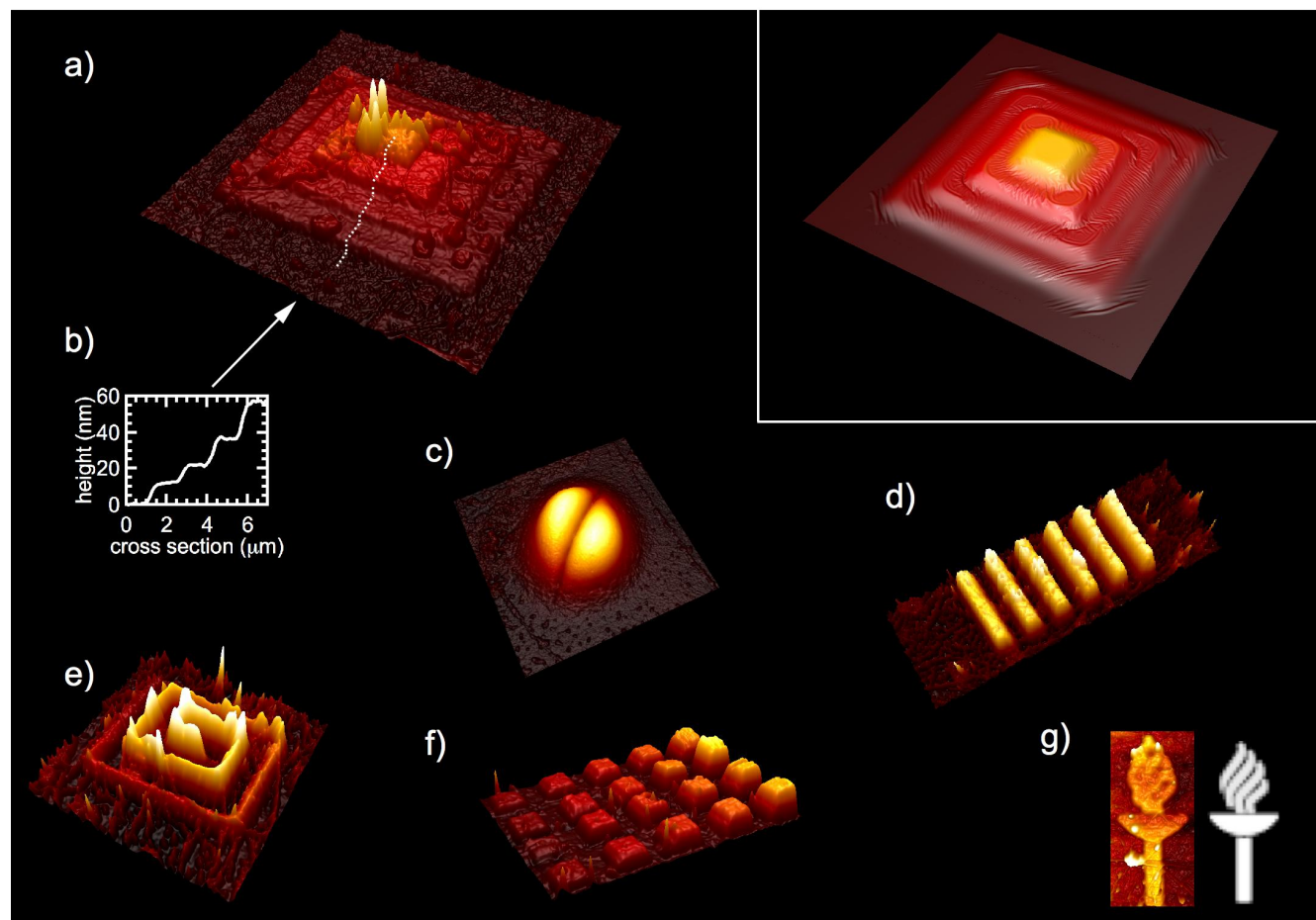


Figure 5. AFM images of 3D structures fabricated by direct laser writing. a) Pyramid structure created by stepwise irradiation of levels. The field of view (FOV) is $17 \times 17 \mu\text{m}^2$. b) Step profile along the dashed line in a. c) 115 nm high semi-sphere which has collapsed symmetrically in the center. FOV is $1.8 \times 1.8 \mu\text{m}^2$. d) Grating structure. FOV is $20 \times 6.7 \mu\text{m}^2$ and the maximum height is 25 nm. e) Chiral structure with continuously increasing height. FOV is $8 \times 8 \mu\text{m}^2$ and the maximum height is 31 nm. f) Matrix of squares. FOV is $19.8 \times 14.7 \mu\text{m}^2$ and the maximum height is 20 nm. g) Torch with the bitmap image (on the right) used for direct laser writing. FOV is $3.5 \times 7.4 \mu\text{m}^2$ and the maximum height is 6 nm. Inset: Simulated pyramid structure with the same dimensions as in a. In the images the z-axis scale has been exaggerated in order to better visualize the structures.

1
2
3
4
5
6 The presented method for forging 2D graphene into 3D shapes opens exciting possibilities for
7
8 further research. For example, shaping graphene into curved structures can be used to generate
9
10 giant pseudomagnetic fields⁵⁻⁷ or to control surface plasmon polaritons.⁸ In addition, we propose
11
12 that 3D structures of graphene can be used for fabricating scaffolds for layered materials,
13
14 suspended device structures, channel networks for nanofluidics, as well as optical and electronic
15
16 devices. Finally, as the formation of 3D structures is simply based on lattice expansion, the
17
18 presented concept is most likely generic to other 2D materials.
19
20
21
22
23

24 ASSOCIATED CONTENT

25 26 27 **Supporting Information**

28
29
30
31 Includes additional Materials and Methods; details on elastic modeling; AFM, Raman and μ m-
32
33 XPS characterization data; and Figures S1-S6.
34
35

36 AUTHOR INFORMATION

37 38 **Corresponding Author**

39
40
41
42 *E-mail: mika.j.pettersson@jyu.fi
43
44

45 **Author Contributions**

46
47
48 M. P. planned the experiments, coordinated and supervised the work and wrote the main part of
49
50 the manuscript. A. J. planned the experiments and the sample fabrication, conducted AFM
51
52 measurements and data analysis, as well as optical imaging. P. M. designed and developed the
53
54 laser setups, performed most of the direct laser writing experiments and did the data analysis. P.
55
56
57
58
59
60

1
2
3 K. planned the simulations, wrote the computer codes, performed the simulations, did the data
4 analysis and wrote the computational part of the manuscript. J. A. built a part of the laser writing
5 setup and performed initial laser writing experiments. J. K. and H. C. T. performed Raman
6 measurements. V. M. H. and J. J. M. performed sample fabrication and characterization. W. Y.
7 W. planned and supervised XPS measurements and analysis. H. C. T., L. Y. C. and C. H. C.
8 conducted XPS measurements and analysis. All the authors discussed the results and commented
9 on the manuscript. †These authors contributed equally to this work.
10
11
12
13
14
15
16
17
18
19

20 Notes

21
22 The authors declare no competing financial interest.
23
24
25

26 ACKNOWLEDGMENTS

27
28 We thank Gerrit Groenhof for reading and commenting the manuscript and Kevin Roberts for
29 help in sample fabrication. P. K. acknowledges the Academy of Finland for funding. W. Y. W.
30 acknowledges funding from Ministry of Science and Technology of the Republic of China
31 (MOST 106-2112-M-008-003-MY3).
32
33
34
35
36
37
38
39
40
41

42 REFERENCES

- 43
44
45
46 (1) Ferrari, A. C.; et al. *Nanoscale* **2015**, 7 (11), 4598–4810.
47
48
49 (2) Franklin, A. D. *Science* **2015**, 349 (6249), aab2750.
50
51
52 (3) Bao, Q.; Loh, K.-P. *ACS nano* **2012**, 6 (5), 3677–3694.
53
54
55 (4) Deng, S.; Berry, V. *Materials Today* **2016**, 19 (4), 197–212.
56
57
58
59
60

- 1
2
3 (5) Guinea, F.; Katsnelson, M. I.; Vozmediano, M. A. H. *Phys Rev B* **2008**, *77* (7), 075422.
4
5
6 (6) Guinea, F.; Katsnelson, M. I.; Geim, A. K. *Nat Phys* **2010**, *6* (1), 30–33.
7
8
9 (7) Levy, N.; Burke, S. A.; Meaker, K. L.; Panlasigui, M.; Zettl, A.; Guinea, F.; Castro Neto,
10 A. H.; Crommie, M. F. *Science* **2010**, *329* (5991), 544–547.
11
12
13 (8) Smirnova, D.; Mousavi, S. H.; Wang, Z.; Kivshar, Y. S.; Khanikaev, A. B. *ACS*
14 *Photonics* **2016**, *3* (5), 875–880.
15
16
17 (9) Bunch, J. S.; Verbridge, S. S.; Alden, J. S.; Van Der Zande, A. M.; Parpia, J. M.;
18 Craighead, H. G.; Mceuen, P. L. *Nano Lett* **2008**, *8* (8), 2458–2462.
19
20
21 (10) Lu, J.; Castro Neto, A. H.; Loh, K.-P. *Nature Communications* **2012**, *3*, 823.
22
23
24 (11) Boddeti, N. G.; Liu, X.; Long, R.; Xiao, J.; Bunch, J. S.; Dunn, M. L. *Nano Lett* **2013**, *13*
25 (12), 6216–6221.
26
27
28 (12) Blees, M. K.; Barnard, A. W.; Rose, P. A.; Roberts, S. P.; McGill, K. L.; Huang, P. Y.;
29 Ruyack, A. R.; Kevek, J. W.; Kobrin, B.; Muller, D. A.; Mceuen, P. L. *Nature* **2015**, 1–9.
30
31
32 (13) Mu, J.; Hou, C.; Wang, H.; Li, Y.; Zhang, Q.; Zhu, M. *Science Advances* **2015**, *1* (10),
33 e1500533–e1500533.
34
35
36 (14) Aumanen, J.; Johansson, A.; Koivistoinen, J.; Myllyperkiö, P.; Pettersson, M. *Nanoscale*
37 **2015**, *7* (7), 2851–2855.
38
39
40 (15) Singh, G.; Rice, P.; Hurst, K. E.; Lehman, J. H.; Mahajan, R. L. *Appl Phys Lett* **2007**.
41
42
43 (16) Ferrari, A. C.; Basko, D. M. *Nature Nanotechnology* **2013**, *8* (4), 235–246.
44
45
46
47
48
49
50
51
52
53
54
55
56
57
58
59
60

- 1
2
3 (17) Beams, R.; Cançado, L. G.; Novotny, L. *J. Phys. Cond. Mat.* **2015**, *27* (8), 083002.
4
5
6 (18) Koivistoinen, J.; Sládková, L.; Aumanen, J.; Koskinen, P.; Roberts, K.; Johansson, A.;
7
8 Myllyperkiö, P.; Pettersson, M. *J Phys Chem C* **2016**, *120* (39), 22330–22341.
9
10
11 (19) Johansson, A.; Tsai, H.-C.; Aumanen, J.; Koivistoinen, J.; Myllyperkiö, P.; Hung, Y.-Z.;
12
13 Chuang, M.-C.; Chen, C.-H.; Woon, W. Y.; Pettersson, M. *Carbon* **2017**, *115*, 77–82.
14
15
16 (20) Farrokhi, H.; Zheng, H. Y.; Zhou, W.; Li, Z. L. *Opt. Express* **2012**, *20* (21), 23180–
17
18 23185.
19
20
21 (21) Dong, T.; Sparkes, M.; Durkan, C.; O'Neill, W. *Journal of Laser Applications* **2016**, *28*
22
23 (2), 022202.
24
25
26 (22) Lee, C.; Wei, X.; Kysar, J. W.; Hone, J. *Science* **2008**, *321* (5887), 385–388.
27
28
29 (23) Rasool, H. I.; Ophus, C.; Klug, W. S.; Zettl, A.; Gimzewski, J. K. *Nature*
30
31 *Communications* **2013**, *4*, ncomms3811.
32
33
34 (24) Lucchese, M. M.; Stavale, F.; Ferreira, E. H. M.; Vilani, C.; Moutinho, M. V. O.; Capaz,
35
36 R. B.; Achete, C. A.; Jorio, A. *Carbon* **2010**, *48* (5), 1592–1597.
37
38
39 (25) Ma, J.; Alfè, D.; Michaelides, A.; Wang, E. *Phys Rev B* **2009**, *80* (3), 033407.
40
41
42 (26) Openov, L. A.; Podlivaev, A. I. *Phys. Solid State* **2015**, *57* (7), 1477–1481.
43
44
45 (27) Terrones, H.; Terrones, M.; Hernández, E.; Grobert, N.; Charlier, J.-C.; Ajayan, P. M.
46
47 *Phys Rev Lett* **2000**, *84* (8), 1716–1719.
48
49
50 (28) Lusk, M. T.; Carr, L. D. *Phys Rev Lett* **2008**, *100* (17), 175503.
51
52
53
54
55
56
57
58
59
60

1
2
3 (29) Cartamil-Bueno, S. J.; Steeneken, P. G.; Centeno, A.; Zurutuza, A.; van der Zant, H. S.
4
5 J.; Houri, S. *Nano Lett* **2016**, *16* (11), 6792–6796.
6
7

8
9 (30) Cartamil-Bueno, S. J.; Centeno, A.; Zurutuza, A.; Steeneken, P. G.; van der Zant, H. S.
10
11 J.; Houri, S. *Nanoscale* **2017**, *9* (22), 7559–7564.
12
13
14
15
16
17
18
19
20
21
22
23
24
25
26

27 BRIEFS

28
29
30 We show that optical engineering of defects in graphene can be used to forge complex 3D
31
32 shapes, which may open profoundly new ways to build devices from 2D materials.
33
34
35
36
37
38
39
40
41

42 Table of Contents Graphic

